Optical Vortex Coronagraphy

David M. Palacios[1], G.A. Swartzlander Jr.[2], and D. Mawet[3]
[1]*Jet Propulsion Laboratory, California Institute of Technology*
[2]*The School of Optical Sciences, The University of Arizona*
[3]*Institut d'Astrophysique et de Geophysique, Universite de Liege*

INTRODUCTION

Optical Vortex Coronagraphy is a new type of high contrast imaging technique under investigation for the Terrestrial Planet Finder Coronagraph (TPF-C). An optical vortex coronagraph (OVC) replaces the amplitude mask typically found in a Lyot Coronagraph with a spiral etched phase plate called an optical vortex mask (OVM). Ideally an OVC cancels light from a star over the entire pupil.[1] This allows for higher planet light throughput and a tighter inner working angle. In addition, an OVC is relatively insensitive to low-order wave front aberrations of the entrance pupil.[2] Recent experiments[3] have demonstrated the low-contrast application of an OVC. An achromatic OVM for low-contrast applications has also been proposed.[4] Using a similar technique it may be possible to produce an achromatic OVM suitable for high contrast applications. In this proceeding, we will address the high contrast performance of an OVC limited by the manufacturability of the OVM. An ideal OVM contains a smoothly varying spiral. However, the spiral phase shape of a real OVM will be pixilated by the lithography technique used to etch it. We simulated this effect with a currently manufacturable non-ideal OVM composed of a grid of square, 0.2 μm × 0.2 μm pixels and present the predicted high contrast performance of an OVC.

WHAT IS AN OPTICAL VORTEX?

Vortices are a ubiquitous feature of waves in nature that are known to occur in a variety of physical systems[5–7]. In optical systems, vortices manifest themselves as dark cores of destructive interference that occur at phase singularities. We can use this dark core to attenuate an on-axis star so nearby planets may be detected.[8] An optical vortex embedded in the center of a monochromatic light beam propagating in the z direction may be described by the electric field:[7]

$$E(\rho, \phi, z, t) = A(\rho, z)\exp(im\phi)\exp(i\omega t - ikz) \tag{1}$$

where (ρ, ϕ z) are cylindrical coordinates, $A(\rho, z)$ is a circularly symmetric amplitude function, m is a signed integer known as the topological charge of the vortex, and $k = 2\pi/\lambda$ is the wave number of a monochromatic field of wavelength λ. At any fixed instant of time, the vortex field described by Equation (1) produces helical surfaces of constant phase given by $m\phi - kz = \text{const}$, where m is a signed integer known as the topological charge, which is given by:[7]

$$m = (1/2\pi)\oint \nabla\phi ds \tag{2}$$

where ∇ϕ is the phase gradient and ds is a line enclosing the helical axis of the vortex. Along the axis of this helix (ρ = 0) the amplitude vanishes owing to destructive interference and a dark vortex core is created, i.e., A(0, z) = 0.

Optical vortices may be created by a variety of different methods.[7] The technique most germane to coronagraphy is the use of an OVM, a type of diffractive optical element we will describe in the next section. Optical vortex holograms and sub-wavelength gratings are also promising methods and will be discussed briefly in a later section.

AN OPTICAL VORTEX MASK

An optical vortex is created when a planar (m = 0) monochromatic beam is passed through a transparent diffractive phase mask having a thickness that varies azimuthally. The thickness of an OVM is given by,[9]

$$dz = m\lambda_0 d\phi / 2\pi(n_s - n_0) \tag{3}$$

where λ^0 is the wavelength for which the mask is intended, $d\phi$ is an azimuthal rotation about the center of the OVM (in units of radians), n_s is the refractive index of the substrate, and n_0 is the index of refraction of the surrounding medium. A simulated 3-D plot of an OVM described by Equation (3) is displayed in Figure 1.

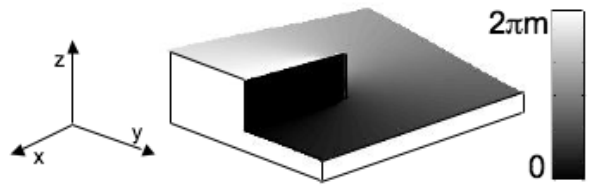

Figure 1: *A three dimensional plot of an optical vortex mask of topological charge m. The thickness of the mask (the z dimension) increases in the azimuthal direction forming a spiral shape on the upper surface of the mask. The thickness of the mask is represented by the phase shift through the mask in radians.*

The light transmitted through an OVM will gain an azimuthally varying phase as stated above, and in addition will also gain a vortex core of zero amplitude along the axis of the helical phase front. The vortex core created by an OVM has a physical extent, not unlike the eye of a hurricane. The vortex core extent may be derived using the simple ray model illustrated in Figure 2.

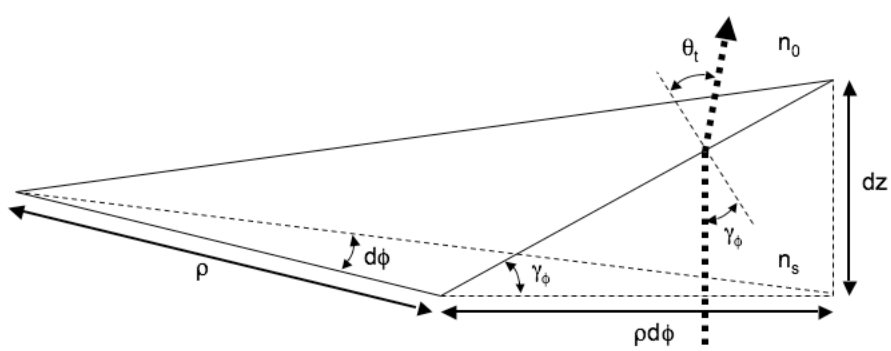

Figure 2: *A ray diagram of light transmission through an azimuthal wedge of an optical vortex mask. The thickness (dz) of the wedge increases as the angular width of the wedge (dφ) increases in the azimuthal direction. A ray (dashed arrow) is perpendicularly incident on the mask at a radial position ρ. The ray is transmitted through the mask substrate of refractive index n_s and is incident on the spiral front surface of the mask at an angle γ_ϕ from the surface normal. The ray refracts at an angle θ_t from the surface normal into the surrounding medium of refractive index n_0.*

The figure depicts a ray perpendicularly incident on the flat backside of the OVM a distance ρ from the center of the mask and at an angle dϕ from the edge of the deepest etch. The ray passes through the OVM glass substrate of refractive index n_s and refracts at the spiral shaped output side of the OVM into the surrounding medium of refractive index n_0. Using geometry it is possible to show that the angle of incidence (γ_ϕ) between the ray and the spiral surface is given by,

$$\gamma_\phi = \tan^{-1}\left[m\lambda_0 / 2\pi\rho(n_s - n_0)\right] \tag{4}$$

Substituting Equation (3) into Equation (4) yields:

$$\gamma_\phi = \tan^{-1}\left[dz/\rho d\phi\right] \tag{5}$$

By examining Equation (5) we can deduce that the closer the ray is to the center of the mask ($\rho \rightarrow 0$) the larger the value of γ_ϕ. The ray will totally internally reflect (TIR) when $\gamma_\phi = \gamma_{TIR} = \sin^{-1}[n_0/n_s]$.[10] It is possible to derive the vortex core size, ρ_c, for an optical vortex created by an OVM by solving for ρ in Equation (5) and setting $\gamma_\phi = \gamma_{TIR}$:

$$\rho_c = m\lambda_0/2\pi(n_s - n_0)\tan[\gamma_{TIR}] \tag{6}$$

All rays incident on the mask within ρ_c totally internally reflect and the transmitted amplitude is zero.

However, this does not completely represent the amplitude transmission of an OVM. When an electromagnetic field is incident on an interface between two dielectric mediums the amplitudes of the reflected and transmitted portions of the field will vary with the angle of incidence and the polarization state of the impinging light.[10] Referring to the geometry depicted in Figure 2, if the electric field is perpendicular to the plane of incidence (defined by the incident ray and the spiral surface) it is radially polarized (E_ρ) and if the electric field is parallel to the plane of incidence it is azimuthally polarized (E_ϕ). The relative amplitude of the transmitted radially polarized light for $\rho > \rho_c$ is given by:

$$\frac{E_\rho}{E_0} = 1 - \frac{n_s\cos(\gamma_\phi) - \frac{\mu_s}{\mu_0}\sqrt{n_0^2 - n_s^2\sin^2(\gamma_\phi)}}{n_s\cos(\gamma_\phi) + \frac{\mu_s}{\mu_0}\sqrt{n_0^2 - n_s^2\sin^2(\gamma_\phi)}} \tag{7}$$

where μ_0 is the magnetic permeability of free space and μ_s is the magnetic permeability of the OVM substrate material. The relative amplitude of the transmitted azimuthally polarized light for $\rho > \rho_c$ is given by:

$$\frac{E_\phi}{E_0} = 1 - \frac{\frac{\mu_s}{\mu_0}n_0^2\cos(\gamma_\phi) - n_s\sqrt{n_0^2 - n_s^2\sin^2(\gamma_\phi)}}{\frac{\mu_s}{\mu_0}n_0^2\cos(\gamma_\phi) + n_s\sqrt{n_0^2 - n_s^2\sin^2(\gamma_\phi)}} \tag{8}$$

Radial line plots of the amplitude transmission of OVMs of topological charge, m = 2, 4, and 6 are compared in Figure 3.

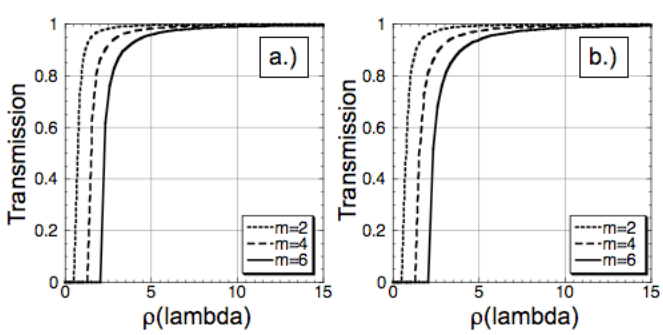

Figure 3: *Radial line plots of the amplitude transmission of optical vortex masks of topological charge, m = 2, 4, and 6 for a) radially polarized light and b) azimuthally polarized light.*

Although the line plots of the radial and azimuthal polarizations seen in Figure 3 look very similar they are slightly different. When linearly polarized light is considered, this leads to a small asymmetry in the vortex core shape. For linear polarized light, the vortex core will be slightly elongated along the axis perpendicular to the

polarization state. This will have a small effect on the performance of the coronagraph that should be noted, although it will be a much smaller effect than the discretization of the OVM.

Previous work on an OVC assumed an ideal OVM with a smooth varying spiral. However, a real OVM will possess a discretized spiral because the etching techniques used to carve the spiral have a minimum etchable feature size. The OVM is a mode converter, and converts the planer non-vortex mode of the telescope into a desired vortex mode of topological charge, m. When the OVM is not manufactured to the desired ideal smooth spiral, the mode conversion will not be complete and other modes of topological charge, $m' \neq m$, will also be created. This includes a non-vortex mode ($m = 0$), which will cause stellar light leakage in the OVC. Using present ion-beam lithography techniques it is possible to etch an $m = 6$ OVM for a wavelength of $\lambda_0 = 600$nm, with a minimum etchable feature size of approximately 50nm.* Due to simulation array size constraints (4096×4096 arrays) the numerical simulations presented in this proceeding contain an OVM with a mask feature size of 0.2 microns.

CORONAGRAPH ARCHITECTURE

A simple unfolded architecture of an OVC is depicted in Figure 4. Light from a distant star is imaged by a telescope represented by L_1. An OVM of topological charge m is placed near the focus of L_1 and a collimator represented by L_2 re-images the entrance pupil of the telescope system after the starlight is transmitted through the OVM. A circular Lyot stop is placed at the re-imaged pupil blocking unwanted starlight at the edge of the pupil. The remaining light is then re-imaged by L_3 with the on-axis starlight greatly attenuated compared to the off-axis light from a planet.

For this proceeding, we assume circular instead of elliptical symmetry since the present TPF-C telescope design contains beam-circularizing optics to increase the efficacy of the wave-front control system. Therefore, ignoring polarization effects, the optimal Lyot stop is a circular aperture.

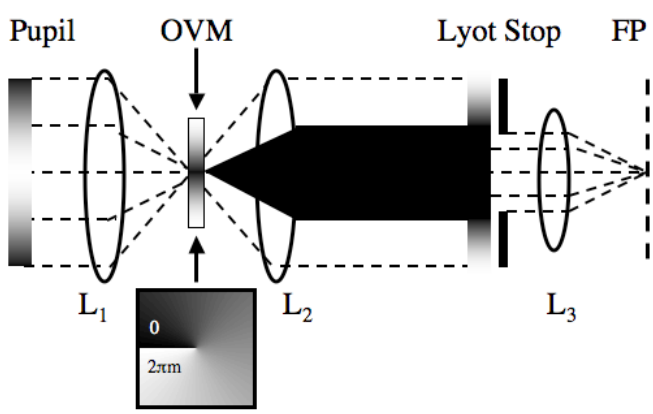

Figure 4: *A simple unfolded model of an optical vortex coronagraph. Lens (L_1) represents the telescope optics, which focus the light from the entrance pupil onto an optical vortex mask (OVM) of topological charge, m. Lens (L_2) collimates the light forming an exit pupil where a Lyot stop is placed. A third lens (L_3) re-images the light to the final image at (FP).*

PERFORMANCE SIMULATIONS

The high contrast performance of an OVC was simulated with an ideal imaging system possessing the following parameters:

- All simulations were performed on a 4096×4096 grid array.
- The OVM was designed to produce either an $m = 2$, 4, or 6 charged vortex at $\lambda_0 = 600$nm.

* Using advanced techniques currently under investigation at JPL it is possible to smooth features without the use of smaller etchable feature sizes.[11-13]

- D=100 pixels.
- The focal spot incident on the OVM was assumed to be an ideal Airy disk with a first zero radius of 51 pixels.
- The star was imaged onto the OVM with an f# = 27 telescope, which matches the design of HCIT at JPL.
- The amplitude transmission function of the OVM was an incoherent superposition of Equation (7) and Equation (8).
- $\mu_s = \mu_0 = 1$.
- $n_s = 1.5$ and $n_0 = 1$.
- The OVM was discretized with a mask feature size of 0.2 microns.
- Contrast as defined by Green[14] et al. was used as a metric of system performance.

Simulated OVC Lyot plane images for an on-axis star are shown in Figure 5.

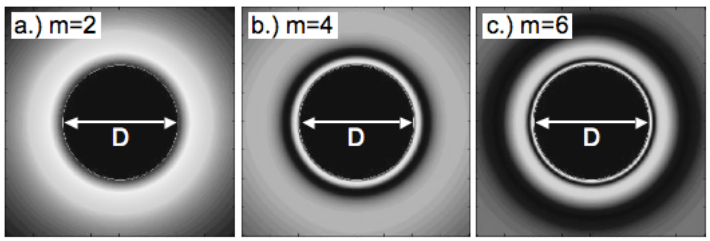

Figure 5: *Images of the Lyot plane of an optical vortex coronagraph with an optical vortex mask of topological charge a) m = 2, b) m = 4, and c) m = 6. The residual stellar light is redistributed outside the pupil of diameter, D.*

One remarkable feature of an ideal OVC is its ability to null over the entire pupil when m is an even integer.[1, 15] The discretization of the OVM causes leakage of stellar light reducing this effect. However, even with the discretized OVM the power inside the pupil was reduced by several orders of magnitude and we were able to verify the Lyot plane intensity profile predicted by Foo et al.[1] (for the m = 2 case) and by Mawet et al.[15]

TPF-C is presently designed to have an inner working angle of 4λ/D. This requires the use of an 8m diameter primary mirror, which is costly and difficult to manufacture. If TPF-C could have an inner working angle of 2λ/D, a 4m diameter primary mirror could be used, which would greatly reduce the cost and difficulty in manufacturing the mirror. Since an OVC is able to null such a large area of the pupil we optimized the performance of the OVC to obtain a contrast below 10^{-10} at 2λ/D. When the OVC contains a discretized OVM the Lyot stop size must be reduced to optimize the system for high contrast performance. The average contrast between 2–3λ/D vs. the Lyot stop diameter is plotted in Figure 6(a) for m = 2, 4, and 6 OVCs.

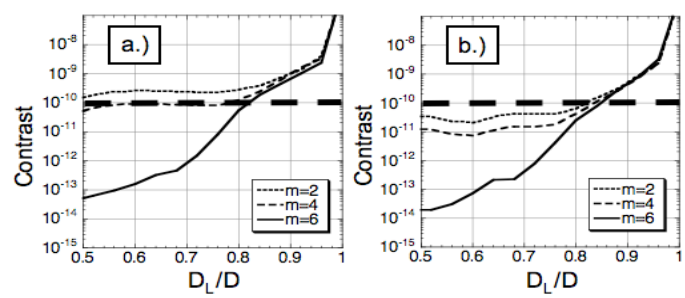

Figure 6: *Plots of the contrast averaged between a) 2–3λ/D and b) 4–5λ/D vs. Lyot stop diameter, D_L, for optical vortex coronagraphs of topological charge, m = 2, 4, and 6. The Lyot stop diameter is normalized by the pupil diameter, D. The thick dashed line at 10^{-10} represents the contrast requirement of the Terrestrial Planet Finder Mission.*

Using these results, we may conclude that a contrast below 10^{-10} at 2λ/D may be obtained by an m = 4 or m = 6 OVC by reducing the Lyot diameter to 0.8D. To compare these results to other coronagraph architectures, the average contrast between 4–5λ/D vs. the Lyot stop diameter is plotted in Figure 6(b). The results show a similar trend although better starlight suppression is obtained in general and now the m = 2 OVC performs better than the required 10^{-10} contrast required for terrestrial planet detection.

Another important quantity to consider is the amount of planet light that is transmitted through the system to the final image plane. A coronagraph may obtain high levels of contrast between a star and a planet but still fail to detect a planet because so few planet photons make it through the system. Besides this minimum detectable signal limitation, it is always desirable to increase the signal from the planet because this will decrease the image integration time. This increases the scientific gain that may be achieved within the mission's lifetime. Planet light throughput may be defined as the amount of planet light power transmitted through the Lyot stop. It's reduced primarily from the Lyot stop but may also be reduced by the on-axis vortex core as well. As a result, the planet light throughput will decrease for OVCs that employ higher m value OVMs, because the size of the vortex core increases with topological charge (see Fig. 3). The planet light throughput vs. Lyot stop size for m = 0, 2, 4, and 6 OVCs are plotted in Figure 7 for (a) a planet/star separation of 2λ/D and (b) a planet/star separation of 4λ/D.

The m = 0 plot in Figure 7 is the no OVM case and represents the maximum power the Lyot stop alone will allow through the system. These results verify our expectation that the planet light throughput decreases as the value of m increases. The plots also show that the Lyot stop throughput itself is the dominant degrader of planet light throughput for smaller Lyot stop sizes. For an m = 4 OVC with $D_L = 0.8D$, a planet separated from its host star by 2λ/D had a throughput of $0.53P_T$, where P_T is the total planet light power. A planet separated from its host star by 4λ/D had a throughput of $0.62P_T$.

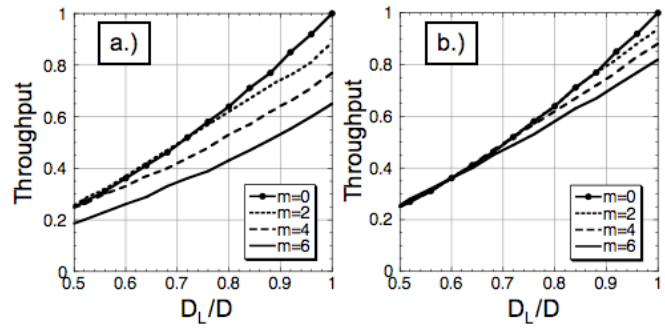

Figure 7: *Plots of the planet light throughput for a planet located at a) 2λ/D and b) 4λ/D vs. Lyot stop diameter, D_L, for optical vortex coronagraphs of topological charge, m = 0, 2, 4, and 6. The Lyot stop diameter is normalized by the pupil diameter, D. The m = 0 case represents the throughput limited by the Lyot stop without an optical vortex mask present.*

VORTEX MASK ACHROMATIZATION

In the search for terrestrial planets few photons may be wasted since the planet signal is so faint. Consequently, TPF-C is required to have a large operating spectral bandwidth to enhance the detected signal. In order for an OVC to be a feasible solution for TPF-C an achromatic design must be implemented. The topological charge imposed by an OVM on light having an arbitrary vacuum wavelength, λ, may be determined from the expression

$$m(\lambda) = m_0 \frac{\lambda_0}{\lambda}\left[\frac{n_s(\lambda) - n_0(\lambda)}{n_s(\lambda_0) - n_0(\lambda_0)}\right] \tag{9}$$

Equation (9) is a dispersive relation, showing that the topological charge varies continuously with the wavelength of the beam. If material dispersion can be ignored, $m(\omega) = m_0\omega/\omega_0$ and thus the vortex spectrum is given by $C_l(\omega) = sinc(m_0\pi\omega/\omega_0 - l\pi)$.[16] If $|\omega - \omega_0|/\omega_0 << 1$, or equivalently $|\lambda - \lambda_0|/\lambda_0 << 1$, the zero-order topological spectrum (corresponding to a non-circulating transmitted field) may be written $C_0^2(\omega) \approx (\delta\lambda/\lambda_0)^2$, where $\delta\lambda = \lambda - \lambda_0$. Thus, when the wavelength is mismatched from λ_0, a fraction of the transmitted beam is unaffected by the OVM.

Achromatic optical components may be created by combining elements that have different refractive properties. An achromatic OVM requires the condition $m(\lambda) = m_0$ to be satisfied across a wide bandwidth of wavelengths. Using Equation (9) the achromatic condition may be expressed $m(\lambda)/m_0 = 1$. The successful fabrication of an achromatic OVM for use in the vicinity of λ_0 therefore depends on finding suitably matched materials.

Toward this end the refractive index may be expressed as a truncated Taylor series expansion:

$$n(\lambda) = n(\lambda_0) + n'(\lambda_0)(\lambda - \lambda_0) + (1/2)n''(\lambda_0)(\lambda - \lambda_0)^2 \tag{10}$$

where $n'(\lambda_0) = \left(\partial n / \partial \lambda\right)\Big|_{\lambda_0}$ and $n''(\lambda_0) = \left(\partial^2 n / \partial \lambda^2\right)\Big|_{\lambda_0}$. For many optical glasses the first two terms in Equation (10) are sufficient to describe the refractive index in the vicinity λ_0 across a bandwidth of roughly 100 nm. Combining Equation (9) and Equation (10) the achromatic condition may be written as an error parameter

$$\varepsilon = \left(n_s - n_0\right)_{\lambda_0} - \lambda_0\left(n_s' - n_0'\right)_{\lambda_0} + (1/2)(\delta\lambda)^2\left(n_s'' - n_0''\right)_{\lambda_0} \tag{11}$$

where $\varepsilon = 0$ satisfies the condition $m(\lambda)/m_0 = 1$. The first term in Equation (10) cannot be made equal to zero; otherwise $\Delta z = \infty$ (see Equation (3)). In practice the value of Δz should be made smaller than the characteristic diffraction length of the beam. Setting $\delta\lambda = 0$, a pair of materials that satisfies $\varepsilon \approx 0$ at a single wavelength, λ_0, may be explored. For optical glasses the second term in Equation (10) is on the order of 10^{-2} and thus the index difference between the glasses must also be small. This difference will result in small Fresnel reflections at the interface, but will also require a value of Δz on the order of $100\lambda_0$. To obtain smaller values of Δz other materials must be explored. Dispersion equations such as the Sellmeier formula may be used to determine the refractive index and its derivatives for a given material. An analysis of more than 100 Schott glasses shows the trend, $|\varepsilon| \approx 1.2 \times |n_s(\lambda_0) - n_0(\lambda_0)|$. Thus large index differences (which are desirable to achieve small values of Δz) require large achromatic errors for these glasses.

The relative topological charge, $m(\lambda)/m_0$, and the topological transmission spectrum, C_l^2, may be numerically computed across the spectrum for a given pair of glasses. For example Figure 8 shows the values for Schott glasses N-LASF44 and N-SF14, and for the parameters $m_0 = 2$ and $\lambda_0 = 550$ nm.

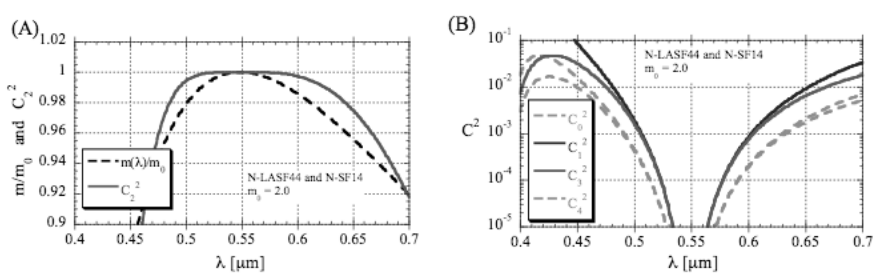

Figure 8: *Achromatic vortex lens having (m_0 =2) at a single wavelength. The matched materials are Schott glasses N-LASF44 and N-SF14. (A) Topological charge and transmission into the intended mode. The integration of $C_2^2(\lambda)$ across a bandwidth of 130 nm indicates that 99.8% of the beam is converted into the $l = m_0 = 2$ mode. (B) Transmission into neighboring modes, indicating no unintended modes at the design wavelength, $\lambda_0 = 550$ nm.*

The bandwidth of the element depends on the fidelity of the transmission into the desired mode, m_0. For example, the 99.8% bandwidth, $\lambda_{max} - \lambda_{min}$, may be established by use of the integral

$$\left(\lambda_{\max} - \lambda_{\min}\right)^{-1} \int_{\lambda_{\min}}^{\lambda_{\max}} C_{m_0}^2 \, d\lambda = 0.998 \tag{12}$$

The data in Figure 8 has a 99.8% bandwidth of 130 nm. In comparison, the 99.8% bandwidth of a chromatic fused silica vortex phase mask in air is 20 nm. As expected, Figure 8(B) shows no transmission into neighboring modes ($l \neq 2$) at λ_0.

OTHER VORTEX CORONAGRAPH ARCHITECTURES

The benefits of an OVC: high planet light throughput, low sensitivity to aberrations, tight inner working angle, are properties inherent to vortex fields and are not dependent on the vortex creation method. However, achromatization and mask manufacturability concerns will depend on the vortex creation method. Above we have explored vortex creation by a helical phase plate, but there are two other optical vortex creation techniques that have been proposed as OVM alternatives. They are the annular groove phase mask (AGPM) and the holographic vortex mask (HVM).

ANNULAR GROOVE PHASE MASK

It is possible to use a diffractive grating instead of a phase plate to induce the helical phase structure of an optical vortex. When the period of a grating is smaller than the wavelength of the incident light, it does not diffract as a classical spectroscopic grating. Instead, all the incident energy is forced to propagate only in the zeroth order, leaving the incident wave front free from any further aberration. This type of grating behaves like a homogeneous medium with unique characteristics that can be used to synthesize birefringent achromatic waveplates. The key point is that by carefully controlling the geometry of the grating structure, one can tune the form of birefringence and induce a precise phase shift between the orthogonal polarization components of the incident light. The phase shifting optical function can then be integrated on the surface of a substrate to implement the phase shifting spatial distribution of an AGPM[15] as shown in Figure 9(A).

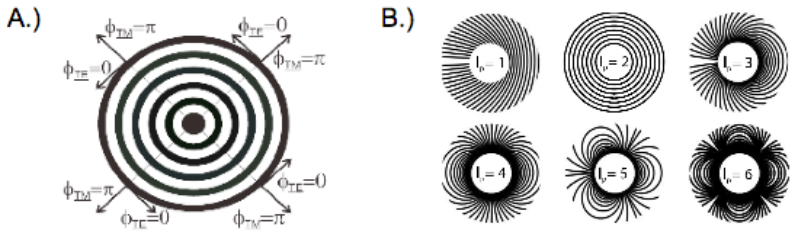

Figure 9: *A) m = 2 AGPM implementation. The AGPM consists of a concentric circular surface-relief grating with rectangular grooves with depth h and a periodicity Λ. B) grating geometry for different topological charges (1–6).*

This technique has been explored in depth for application in the infra-red requiring 10^{-6} starlight suppression.[15] However, to apply this technique to TPF-C, a high topological charge AGPM as shown in Figure 9(B) would have to be developed for use in visible light. High topological charged AGPM coronagraphs for the visible spectrum are still under development.

HOLOGRAPHIC VORTEX MASK

It is also possible to create an optical vortex with a hologram,[7] which may be created by interfering the desired vortex beam with a plane wave. The resulting intensity pattern (see Fig. 10(A)) is then etched onto a substrate to produce a holographic diffraction grating.

To further improve the design the holographic mask may be etched directly onto a prism creating a vortex grism. This device is inherently broadband because the same topological charged vortex is produced for all wavelengths and the prism compensates for the angular dispersion of the diffraction orders. A possible coronagraph concept making use of this technique is depicted in Figure 10(B). This technique holds several advantages over a helical OVM. First it is inherently broadband and second, it doesn't require the lithographic etches to penetrate as deep into the mask substrate. This technique is currently under investigation.

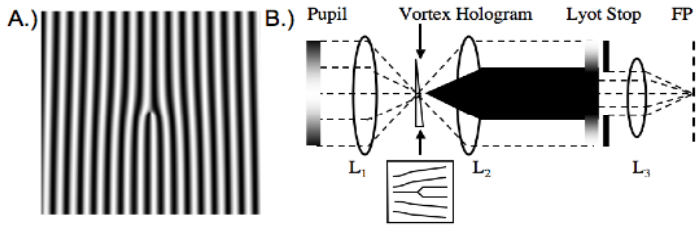

Figure 10: *A) An m = 1 vortex hologram. B) A holographic vortex coronagraph employing a vortex grism.*

CONCLUSIONS

An OVC employing an optical vortex mask etched by today's ion-beam technology is able to achieve the 10 order of magnitude starlight suppression required of TPF-C. Our simulations verify the Lyot plane behavior of an OVC predicted by Foo et al.[1] and Mawet et al.[15] An m = 4 OVC with $D_L = 0.8D$, reached the required 10^{-10} starlight suppression and obtained a planet light thoughput of $0.53P_T$ for a planet separated from its host star by $2\lambda/D$. An OVC may hold several key advantages for TPF-C. These advantages include high planet light throughput, manufacturability, lower aberration sensitivity,[2] and possible broadband operation.[4] Vortex masks with topological charge ranging from m = 1–3 have been manufactured.[12,13] Using present ion-beam lithography techniques, it may be possible to construct an m = 6 vortex mask designed for an optical wavelength of $\lambda_0 = 600$nm. In addition, alternative architectures may relax achromatic OVC design tolerances. Two alternative architectures have been suggested, the annular groove phase mask and the holographic vortex coronagraph, both of which are presently under investigation.

ACKNOWLEDGMENTS

David M. Palacios would like to thank S. Shaklan and D. Wilson for their suggestions and comments. This work was carried out at: the Jet Propulsion Laboratory, California Institute of Technology, under contract with the National Aeronautics and Space Administration, the University of Arizona supported by a grant from the U.S. Army Research Office, and at the University of Liege.

REFERENCES

1. G. Foo, D.M. Palacios, G.A. Swartzlander Jr., Opt. Lett. **30**, 3308 (2005).
2. D.M. Palacios and S. Hunyadi, To appear in Optics Letters (2006).
3. Jae Hoon Lee, Gregory Foo, Eric G. Johnson, and Grover A. Swartzlander Jr., Phys. Rev. Lett. Article # 053901 (2006).
4. G.A. Swartzlander Jr., Opt. Lett. **31**, 2042 (2006).
5. L.M. Pismen, *Vortices in Nonlinear Field*s, Oxford Science Publications (Clarendon Press, Oxford, 1999).
6. Sheldon Green eds., *Fluid Vortices*, (Kluwer Academic Publishers, Dordrecht, Netherlands, 1995).
7. M. Vasnetsov and K. Staliunas, eds., *Optical Vortices*, vol. 228, Horizons in World Physics, (Nova Science, Huntington, NY, 1999).
8. G.A. Swartzlander Jr., Opt. Lett. **26**, 497 (2001).
9. F.B. Colstoun, G. Khitrova, A.V. Fedorov, T.R. Nelson, C. Lowery, T.M. Brennan, B.G. Hammons, and P.D. Maker, Chaos, Solitons, & Fractals **4**, 1575 (1995).
10. J.D. Jackson, *Classical Electrodynamics*, (John Wiley and Sons, NY, 1962).
11. D. W. Wilson, R. E. Muller, P. M. Echternach, and J. P. Backlund, Proceedings of SPIE, **5720**, 68 (2005).
12. Z. G. Chen, M. Segev, D. W. Wilson, R. E. Muller, and P. D. Maker, Opt. Lett. **22,** 1751 (1997).
13. Z. G. Chen, M. Segev, D. W. Wilson, R. E. Muller, and P. D. Maker, Phys. Rev. Lett. **78**, 2948 (1997).
14. Green, J.J., and Shaklan, S.B., Proc. SPIE **5170**, 25 (2003).
15. D. Mawet, P. Riaud, O. Absil, and J. Surdej, ApJ. **633**, 1191 (2005).
16. G.A. Swartzlander Jr., Opt. Lett. **30**, 2876 (2005).